# PROPELLER DESIGN AND ANALYSIS FOR PEDAL DRIVEN AND OTHER ODD AIRCRAFT

E. Eugene Larrabee and Susan French
Massachusetts Institute of Technology
Cambridge, Massachusetts

Presented at the XVIIth OSTIV Congress
Paderborn, Germany
May 1981

## ABSTRACT

A simple theory of the lifting line type has been developed for the design of high efficiency rotors (propellers and horizontal axis windmills), the prediction of their off-design performance, and the performance of arbitrary rotors generally. Although the design calculations can be carried out with a pocket scientific calculator, the off-design and arbitrary rotor performance calculations are more conveniently performed with a small programmable digital computer. A FORTRAN IV code named HELICE, which will run on a PDP 10/11 computer, has been written at M.I.T. by Mrs. Susan French for this purpose. This paper discusses the algorithms used in HELICE and its application to the design and performance prediction of propellers for: 1. a Wakefield class rubber model; 2. a powered hang glider; 3. a self-launching sailplane; and 4. a pedal driven airplane. An earlier version of this procedure was used to design propellers for M.I.T.'s Chrysalis and Paul MacCready's Gossamer Albatross human powered airplanes.

## INTRODUCTION

The first lifting line analysis of minimum induced loss propellers[1] was published by Betz (with an appendix by Prandtl) at Goettingen in 1919. Sydney Goldstein's 1929 doctor's dissertation, also done at Goettingen[2], may be regarded as confirming the essential correctness of the approximate radial circulation distributions corresponding to minimum induced loss operation calculated by Betz and Prandtl. Glauert seems to have been on the verge of publishing a related propeller momentum theory consistent with these minimum induced loss concepts in 1934, but his untimely death may have prevented him from writing it down correctly[3]. Since then other investigators have considered related theories, e.g. Lerbe[4], Theordorsen[5], Hirsch[6], Giordano[7], and de Vries[8], each with varying degrees of elaboration and specialization, but the one given below is conceptually very simple, and has given predictions which agree well with experimental data[9,10] for low solidity rotors operated at low advance ratios ($V/\Omega R < 0.5$).

## THE BETZ CONDITION

Betz said[1]: "Die Stroemung hinter einer Schraube mit geringstem Energieverlust ist so, wie wenn die von jeden Schraubenfluegel durchlaufene Bahn (Schruabenflaeche) erstarrt waere und sich mit einer bestimmten Geschwindigkeit nach hinten verscheibt, oder sich mit einer bestimmten Winkelgeschwindigkeit um die schraubenachse dreht" (The flow behind a screw of minimum energy loss is as if the path [helicoidal surface] laid down

by each blade were made rigid and displaced itself toward the rear with a certain [axial] velocity, or turned itself about the screw axis with a certain angular velocity). This is Betz's "rigid wake" condition, and thinking of the idealized helicoidal vortex sheets as moving rigid bodies is exactly what has confused rotor analysts for 60 years, since idealized "free" vortex sheets cannot move as rigid bodies; but they do move locally perpendicular to themselves and they can give the appearance of rigid body motion if the local sheet velocity is given by $v' \cos\phi$, where $v'$ is the radially uniform Betz "displacement" velocity and $\phi$ is the local helix angle, measured from a plane perpendicular to the screw axis. This is shown in Figure 1.

It follows that the axial velocity and the rotational velocity of a helicoidal vortex sheet, moving so as to satisfy the Betz condition, is given by (I use Glauert's notation throughout):

$$w_{axial} = v' \cos^2\phi \qquad (1)$$

$$w_{rotational} = v' \cos\phi \sin\phi \qquad (2)$$

To show that this vortex sheet motion minimizes the induced loss of a lightly loaded rotor, consider Figure 2 which shows the components of the local velocity acting on a propeller blade element, and the associated lift and drag (or thrust and torque) components of its loading.

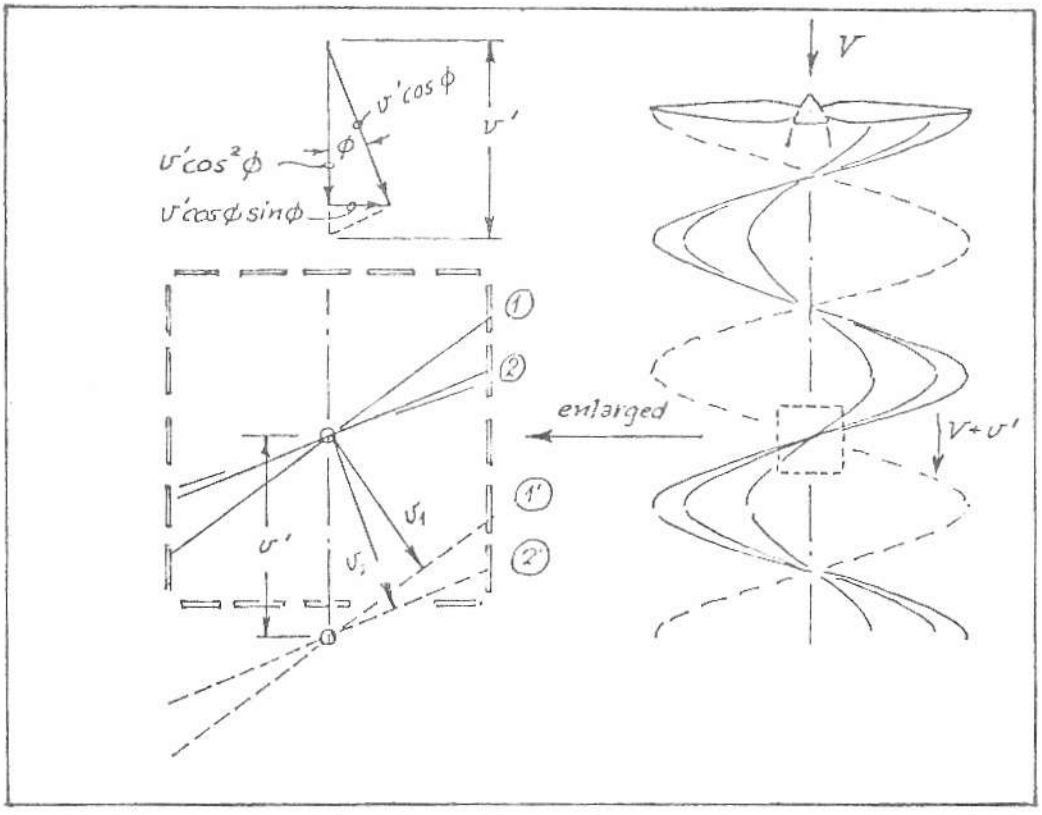


Fig. 1 Helicoidal vortex sheet motion to fulfill the Betz condition. Helical vortex filaments 1 and 2 appear to move axially with the displacement velocity, v', but actually move perpendicular to themselves with velocities $v_1$ and $v_2$.

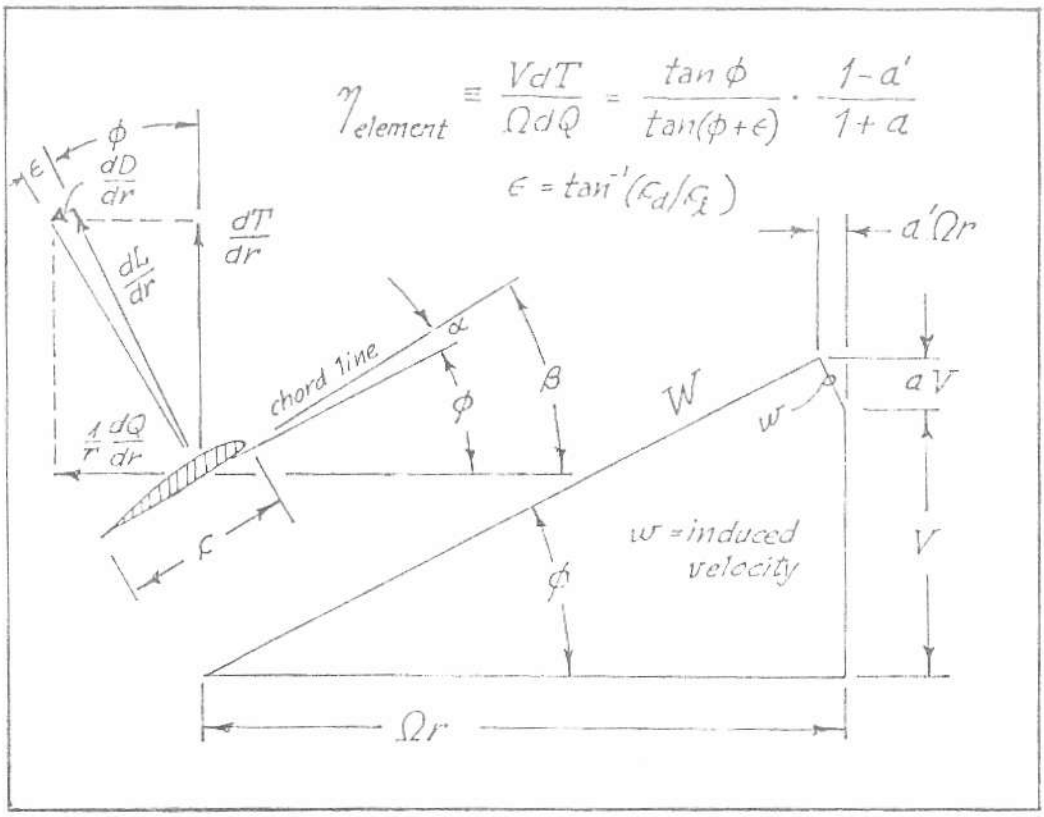


Fig. 2 Blade element velocity diagram and loading in Glauert's notation.

The blade element efficiency is given by

$$\eta_{\substack{\text{propeller}\\\text{element}}} = \frac{VdT}{\Omega dQ} = \frac{\tan\phi}{\tan(\phi+\epsilon)} \cdot \frac{1-a'}{1+a} \quad (3)$$

$$= \eta_{profile} \cdot \eta_{induced} \quad )a)$$

where $\phi$ is the helix angle of the blade velocity vector W, $\epsilon = \tan^{-1}(\frac{c_d}{c_l})$, V is the flight velocity, $\Omega$ is the shaft velocity, and a and a' are dimensionless measures of aV and a'$\Omega$r, the axial and rotational components of the induced velocity, w.

If the propeller is lightly loaded

$$\eta_{induced} \equiv \frac{(1-a')}{(1+a)} \equiv \frac{1}{1+a+a'} \quad (4)$$

and if the induced velocity components are half the vortex sheet velocity (exactly as in wing theory), one obtains

$$a = \frac{1}{2}\frac{v'}{V}\cos^2\phi \equiv \frac{1}{2}\frac{v'}{V}\frac{(\Omega r)^2}{(\Omega r)^2 + V^2} \quad (5)$$

$$a' = \frac{1}{2}\frac{v'}{\Omega r}\cos\phi\sin\phi = \frac{1}{2}\cdot\frac{v'}{V}\cdot\frac{V}{\Omega r}\cdot\frac{\Omega r\cdot V}{(\Omega r)^2 + V^2} \quad (6)$$

Substituting equations 5 and 6 in equation 4 gives

$$\eta_{induced} \equiv \frac{1}{1+\frac{1}{2}\frac{v'}{V}} \quad (7)$$

which is maximized for the propeller as a whole if v'/V is radially constant. This argument is due to Glauert[3]. A similar argument applies to a windmill or "ram air turbine" blade element whose

efficiency is the exact inverse:

$$\eta_{\substack{\text{windmill}\\ \text{element}}} = \frac{\Omega dQ}{V dT} = \frac{\tan(\phi+\varepsilon)}{\tan\phi} \cdot \frac{1+a}{1-a'} \quad (8)$$

here Q, T, $\varepsilon$, a, a' and v' are all negative.

## THE BENTZ-PRANDTL AND GOLDSTEIN CIRCULATION DISTRIBUTIONS COMPARED

To find the circulation distribution bound to each of B rotor blades at radius r for the vortex sheet motion satisfying the Betz condition, Stoke's Law is applied to an annular tube of radially undisturbed slipstream (light loading assumed) lying between a radius r and the outer radius R (equal to the propeller radius), whence:

$$B\Gamma = 2\pi r \cdot \bar{w}_{\text{rotational}} \quad (9)$$

The average rotational velocity $w_{\text{rotational}}$ at radius r will differ from the sheet rotational velocity, v' $\cos\phi \sin\phi$ [where $\phi \cong \tan^{-1}\left(\frac{V}{\Omega r}\right)$] by a factor F, which Prandtl estimated from an analogy with the known solution in two dimensional flow for the average velocity of fluid within an infinite array of semi-infinite plates spaced a distance s apart and moving perpendicular to themselves. If y is the distance from the plate edges, and v is their common velocity [see Ref. 3],

$$v_{\text{average}} = F \cdot v = \frac{2}{\pi} \cos^{-1}(e^{-f}) \quad (10)$$

where

$$f = \pi(y/s) \quad (11)$$

The corresponding value of f (the edge distance-sheet spacing parameter) for the flow near the edges of an array of helicoidal vortex sheets moving with velocity v' $\cos\phi$ is

$$f = \frac{B}{2} \cdot \frac{\sqrt{\lambda^2+1}}{\lambda} \cdot (1 - \frac{r}{R}) \quad (12)$$

where $\lambda$, the advance ratio is

$$\lambda = V/\Omega R \quad (13)$$

solving equation 9 for $\Gamma(r)$, introducing the velocity fraction F, and rearranging allows us to write an approximate analytic expression for the dimensionless bound circulation corresponding to minimum induced loss:

$$\frac{B\Omega\Gamma}{2\pi V v'} \equiv G = \frac{Fx^2}{x^2+1} \quad (14)$$

where

$$x = \Omega r/V = (r/R)/\lambda = \xi/\lambda \quad (15)$$

$$F = (2/\pi) \cos^{-1}(e^{-f}) \quad \text{(10) repeated}$$

$$F = (B/2)(\sqrt{\lambda^2+1}/\lambda)(1-\xi) \quad \text{(12) repeated}$$

The symbol G for this normalized circulation is chosen in honor of Glauert and Goldstein. Values of G calculated by equation 14 are plotted as a function of $r/R = \xi$ for two and four blade rotors operating at $\lambda = 0.2$ and 0.5 in Figure 3. Goldstein's painfully calculated more exact results[2] are included for comparison. The quantity s/R on the curves is the ratio of the perpendicular edge spacing of the vortex sheets to the propeller tip radius. I draw the conclusion that the Betz-Prandtl approximate minimum induced loss circulation is valid if s/R is less than one. At higher values of s/R the Betz-Prandtl distribution would require heavier blade loading at large radii and lighter loading at small radii, a modification which might even be desirable from a practical standpoint!

The quantity G has a momentum interpretation as well. Since $x^2/(x^2+1) \cong \cos^2\phi$, G is equal to the ratio of the average axial velocity in the slipstream at radius r to the displacement velocity, v'. If a single rotation propeller could become an "actuator disc", G would equal 1 at all $r < R$, which would require $B \to \infty$ and

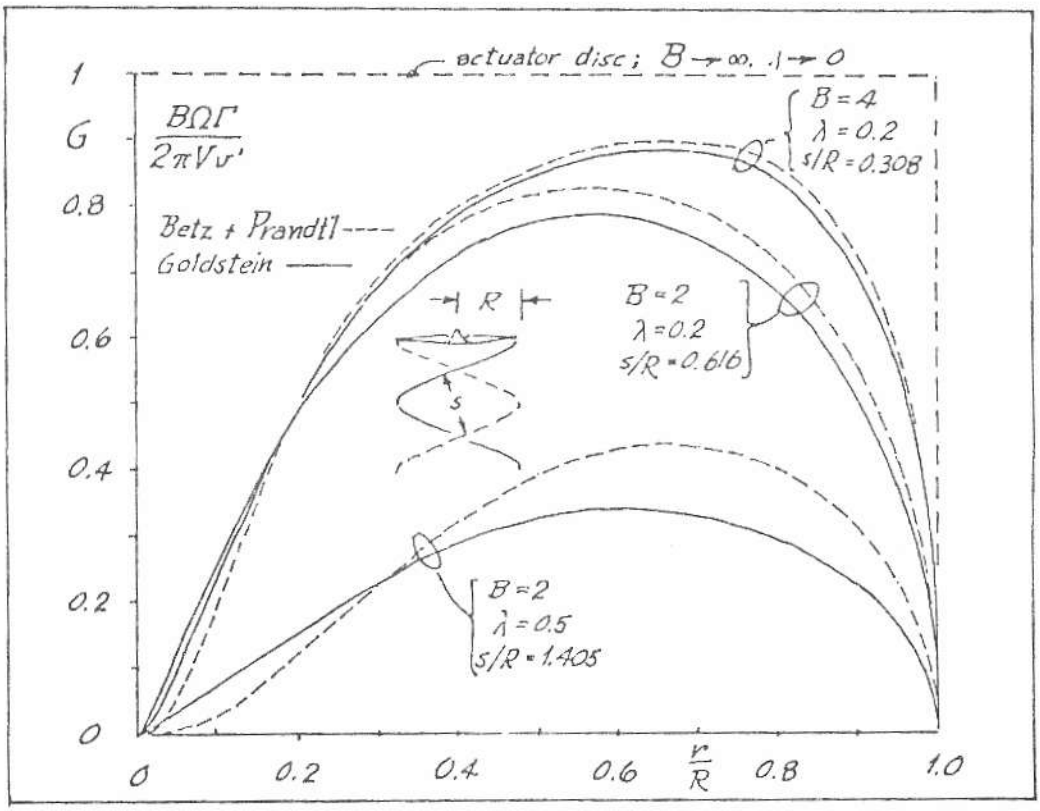


Fig. 3 Minimum induced loss bound circulation according to Betz and Prandtl -- and according to Goldstein.

$\lambda \to 0$. High pitch propellers with a small number of blades will always have higher induced losses than many-bladed flat pitch propellers because of the inherently more periodic nature of their slipstream flow.

## COMPUTER DESIGN OF PROPELLERS OF HIGHEST EFFICIENCY

On the other hand, the profile efficiency, $\tan\phi/\tan(\phi + \varepsilon)$, is maximized if $\phi = \frac{\pi}{4} - \frac{\varepsilon}{2}$, which would require that $\varepsilon$ be made as small as possible, and that the most heavily loaded blade elements operate at $\phi \cong 45^\circ$, corresponding to $\lambda \cong 1$. Also, smaller blade numbers will increase the blade chords required to maintain the nearly constant propeller solidity needed to support a given disc loading, leading to higher blade element Reynolds numbers and reduced values for $\varepsilon$. Therefore, the design of a propeller of highest efficiency for a specified disc loading involves a balancing of the conflicting requirements for high induced efficiency, which favors low advance ratios and a large number of blades, and for high profile efficiency, which favors a high advance ratio and a small number of blades.

The analyst achieves this balance in the HELICE program with a procedure suggested by Goldstein which determines the radially uniform displacement velocity ratio, $\zeta \equiv \frac{v'}{V}$, corresponding to minimum induced loss loading for a given wake geometry, $G(B,\lambda)$, and the associated overall efficiency, corresponding to the expected radial distribution of blade element lift to drag ratio. The procedure follows:

1) Calculate four loading integrals:

$$\frac{dI_1}{d\xi} = 4\xi G\left(1 - \frac{D/L}{x}\right); \quad I_1 = \int_0^1 \frac{dI_1}{d\xi}\, d\xi \text{ , etc.} \tag{16}$$

$$\frac{dI_2}{d\xi} = 2\xi G\left(1 - \frac{D/L}{x}\right)\left(\frac{1}{x^2+1}\right) \tag{17}$$

$$\frac{dJ_1}{d\xi} = 4\xi G \left[1 + \left(\frac{D}{L}\right)x\right] \quad (18)$$

$$\frac{dJ_2}{d\xi} = 2\xi G \left[1 + \left(\frac{D}{L}\right)x\right] \left[\frac{x^2}{x^2+1}\right] \quad (19)$$

2) If thrust is specified, $T_c \equiv \frac{2T}{\rho V^2 \pi R^2}$

$$\zeta = \frac{I_1}{2I_2}\left[1 - \sqrt{1 - \frac{4T_c I_2}{I_1^2}}\right] \quad (20)$$

$$P_c \equiv \frac{2P}{\rho V^3 \pi R^2} = J_1\zeta + J_2\zeta^2 \quad (21)$$

$$\eta = T_c/P_c \quad (22)$$

3) If power is specified, $P_c = \frac{2P}{\rho V^3 \pi R^2}$

$$\zeta = \frac{J_1}{2J_2}\left[\sqrt{1 + \frac{4P_c J_2}{J_1^2}} - 1\right] \quad (23)$$

$$T_c = I_1\zeta - I_2\zeta^2 \quad (24)$$

$$\eta = T_c/P_c \quad \text{(22) repeated}$$

Equations 20 and 23 are the rotor lifting line equivalents of the wing lifting line formula for the spanwise constant induced angle of attack corresponding to elliptic loading:

$$\alpha_{induced} = \frac{C_L}{\pi(b^2/S)} \quad (25)$$

The more complicated rotor form is necessary to account for the wake geometry and for the fact that the specified thrust or power depends on the resolution of blade element drag as well as lift into thrust and torque components.

If the propeller efficiency given by this procedure for various trails of B, P (or T), V, $\phi$, R, and $\rho$ seems to be satisfactory, it is a simple matter to determine the corresponding propeller blade geometry. For the case of a fuselage or nacelle so small compared to the propeller that its effect of the flow field can be neglected, the blade element velocity helix angle and magnitude are given by

$$\phi = \tan^{-1}\left[\frac{\lambda}{\xi}\left\{1 + \frac{\zeta}{2}\right\}\right] \quad (26)$$

$$\frac{W}{V} = \sqrt{x^2 + 1 - \left(\frac{1}{2}\zeta\cos\phi\right)^2} \quad (27)$$

The blade angle and chord are given by

$$\beta = \phi + \alpha \quad (28)$$

$$\frac{c}{R} = \frac{4\pi\lambda}{B} \cdot \frac{G}{W/V} \cdot \frac{\zeta}{c_\ell} \quad (29)$$

where $\alpha$ and $c_\ell$ are the blade element design angle of attack and lift coefficient in "two dimensional" flow corresponding to the values of D/L used to calculate the blade loading integrals $I_1$, $I_2$, $J_1$, and $J_2$.

As soon as the blade chord is calculated it becomes possible to calculate the blade element Reynolds number, Mach number, and thickness-to-chord ratio:

$$R_e = \frac{\rho V R}{\mu} \cdot \frac{c}{R} \cdot \frac{W}{V} \quad (30)$$

$$Ma = \frac{V}{a} \cdot \frac{W}{V} \quad (31)$$

$$\frac{t}{c} = \frac{t/R}{c/R} \quad (32)$$

the quantity t/R is presumably limited by structural constraints on strength or

stiffness. Consideration of the effect of these parameters on the blade element characteristics may indicate the desirability of iterating the procedure with improved values of D/L along the radius. Also, the integrals $I_1$, $I_2$, $J_1$, and $J_2$ depend on the light loading assumption that $W/V \cong \sqrt{x^2 + 1}$. If $\zeta$ is large (it is frequently larger than $\lambda$), improved values for the radial gradients of $T_c$ and $P_c$ are given by

$$\frac{dT_c}{d\xi} = 4\zeta\lambda G \left(\frac{W}{V}\right)\left(\cos\phi - \frac{D}{L}\sin\phi\right) \qquad (33)$$

$$\frac{dP_c}{d\xi} = 4\zeta\xi G \left(\frac{W}{V}\right)\left(\sin\phi + \frac{D}{L}\cos\phi\right) \qquad (34)$$

which, on integrating, will turn out to be sligtly different from the values given by equations 21 and 24. Some analysts, Theodorsen, for example[5], would iterate the calculations with values of $G[B,\lambda(1 + \frac{\zeta}{2})]$, but, since experiment shows that the helicoidal vortex sheets actually roll up quickly at the edges for large values of $\zeta$, and that the rolled up tip vortices preserve the light loading helix angle $\tan^{-1}\lambda$ (because the axial velocity increase at the outer edges of the slipstream is very small), there is no reason to suppose that such a modification is a step closer to reality.

On the other hand, when the fuselage or nacelle is large enough to affect the propeller flow field, as it almost invariably is for piston engine installations, the disturbance must be taken into account and the propeller must be "body" or, in the case of steamboats, "wake" adapted, as suggested by Lerbs[4]. If the azimuthally averaged axial velocity to free stream velocity ratio at radius r due to the fuselage or nacelle (in the absence of the propeller) is given by $\bar{u}$, I recommend that the blade angles be calculated as follows:

$$\beta = \tan^{-1}\left[\frac{\lambda}{\xi}\left(\bar{u} + \frac{\zeta}{2}\right)\right] + \alpha \qquad (35)$$

This, in combination with the chords given by equation 29, will tend to preserve the minimum induced loss radial loading. More will be said about the effects of the body on the net propulsive efficiency in a later section.

## OFF-DESIGN AND ARBITRARY ROTOR PERFORMANCE

If it is assumed that the changes in axial and rotational momenta in every annulus of slipstream behind an isolated rotor are due solely to the loads on the blade elements in contact with it, that the average slipstream volocity changes are less than the sheet velocities by Prandtl's factor F, and that the axial and rotational components aV and a'$\Omega$r of the induced velocities are half the "ultimate" sheet velocities, the following approximate equations can be written for the radial gradients of thrust and torque:

$$\frac{dT}{dr} = (2\pi r)\rho V(1 + a)2F(aV)$$

$$= \frac{1}{2}\rho V^2\left(\frac{1 + a}{\sin\phi}\right)^2 Bc(c_\ell\cos\phi - c_d\sin\phi) \qquad (36)$$

$$\frac{1}{r}\frac{dQ}{dr} = (2\pi r)\rho V(1 + a)\,2F\,(a'\Omega r)$$

$$= \frac{1}{2}\rho V^2\left(\frac{1 + a}{\sin\phi}\right)^2 Bc(c_\ell\sin\phi + c_d\cos\phi) \qquad (37)$$

These can be solved for the induced velocity components to yield

$$\frac{a}{1 + a} = \frac{1}{4}\frac{\sigma}{F}\frac{(c_\ell\cos\phi - c_d\sin\phi)}{\sin^2\phi} \qquad (38)$$

$$\frac{a'}{1 + a'} = \frac{1}{4}\frac{\sigma}{F}\frac{(c_\ell\sin\phi + c_d\cos\phi)}{\sin\phi\cos\phi} \qquad (39)$$

where $\sigma \equiv Bc/2\pi r$ is the local rotor solidity. These equations appear incorrectly, with F in the numerator, in Glauert's article[3] written just before his death. Equations 38 and 39 are anlogous to an approximate lifting line theory for wings in which the induced

angle at any spanwise location is assumed to depend only on the local spanwise loading, thus:

$$\alpha_{induced} = \frac{1}{4} \cdot \frac{c/b}{\sqrt{1 - (2y/b)^2}} \cdot c_\ell \qquad (40)$$

Here $\sqrt{1 - (2y/b)^2}$ plays the role of F in equations 38 and 39. If we consider a flat, elliptic planform wing with a spanwise constant $c_\ell = C_L = Lift/qS$, $\frac{c}{b} = (\frac{c_o}{b}) \sqrt{1 - (2y/b)^2}$ and $S = \frac{\pi}{4} c_o b$, we find that equation 40 gives the familiar spanwise constant induced angle of attack,

$$\alpha_{\substack{induced \\ elliptic \\ loading}} = \frac{C_L}{\pi(b^2/S)}$$

Application of equation 40 to arbitrary wings gives plausible spanwise lift distributions which diverge from the more correct Fourier harmonic solutions of Glauert in proportion to their departure from elliptic loading. Many writers have commented on the approximate "radial independence of blade elements" which equations 36 and 37 imply, and how equations 38 and 39 can be expected to be more valid than equation 40.

To find the radial load distribution on a rotor blade, it is convenient to make the characteristics of the blade element airfoils functions of the angle of attack between ±90°, thus:

$-\frac{\pi}{2} < \alpha < \alpha_1$

$$c_\ell = c_{\ell_1} (\cos\alpha/\cos\alpha_1) \qquad (41)$$

$$c_d = |\sin\alpha| \qquad (42)$$

$\alpha_1 \leq \alpha \leq \alpha_2$

$$c_\ell = c_{\ell_1} + \{\frac{c_{\ell_2} - c_{\ell_1}}{\alpha_2 - \alpha_1}\} (\alpha - \alpha_1) \qquad (43)$$

$$c_d = c_{d_3} + [dc_\ell/d(\alpha^2)](\alpha - \alpha_3)^2 \qquad (44)$$

$\alpha_2 < \alpha < \pi/2$

$$c_\ell = c_{\ell_2} (\cos\alpha/\cos\alpha_2) \qquad (45)$$

$$c_d = |\sin\alpha| \qquad (42) \text{ repeated}$$

Such a model of blade element aerodynamics has been found to represent rotor stalling realistically.

To find the load at a given radial station, an initial angle of attack $\alpha_n$ is chosen, and the following quantities are computed:

$$\phi_{n_I} = \beta - \alpha_n \qquad (46)$$

$$c_{\ell_n} = c_\ell(\alpha) \qquad \text{(equations 41,43, or 45)}$$

$$c_{d_n} = c_d(\alpha) \qquad \text{(equations 42 or 44)}$$

$$a_n = a(\sigma, F, \phi_{n_I}, c_{\ell_n}, c_{d_n}) \qquad \text{(equation 38)}$$

$$a'_n = a'(\sigma, F, \phi_{n_I}, c_{\ell_n}, c_{d_n}) \qquad \text{(equation 39)}$$

$$\phi_{n_{II}} = \tan^{-1} \left[ (\lambda/\xi)(1 + a_n) / (1 - a'_n) \right] \qquad (47)$$

$$\phi_{n_I} - \phi_{n_{II}} \qquad (48)$$

The process is then iterated with a new value of $\alpha$

$$\alpha_{n+1} = \alpha_n + \frac{1}{2} (\phi_{n_I} - \phi_{n_{II}}) \qquad (49)$$

until the absolute value of $(\phi_{n_I} - \phi_{n_{II}})$ is less than some small number (e.g. 0.001°) The converged values of $a', \phi, c_\ell$, and $c_d$ are then used to find the radial gradients of the thrust and power coefficients based on the shaft speed at each radial station:

$$\frac{dC_T}{d\xi} = \frac{\pi^3}{4}\left(\frac{1-a'}{\cos\phi}\right)^2 \xi^3 \sigma\,(c_\ell \cos\phi - c_d \sin\phi) \tag{50}$$

$$\frac{dC_P}{d\xi} = \frac{\pi^4}{4}\left(\frac{1-a'}{\cos\phi}\right)^2 \xi^4 \sigma\,(c_\ell \sin\phi + c_d \cos\phi) \tag{51}$$

These are integrated radially to find $C_T$ and $C_P$.

$$C_T \equiv \frac{T}{\rho n^2 D^4} = \int_0^1 \frac{dC_T}{d\xi}\, d\xi; \quad \left\{ \begin{array}{l} n = \Omega/2\pi \\ D = 2R \end{array} \right\}$$

$$C_P \quad \frac{P}{\rho n^3 D^5} = \int_0^1 \frac{dC_P}{d\xi}\, d\xi$$

These may be compared readily with the thrust and power coefficients based on the forward speed, which may have been used in the minimum induced loss rotor design procedure described before, by the following conversions:

$$T_C = \frac{8}{\pi^3}\frac{C_T}{\lambda^2} \tag{52}$$

$$P_C = \frac{8}{\pi^4}\frac{C_P}{\lambda^3} \tag{53}$$

Propeller performance is usually presented in terms of $C_T$ and $C_P$ as functions of the advance ratio, $\lambda$, or the effective pitch/diameter ratio, $J = \pi\lambda$, because there is always a shaft speed even though V may be zero; windmill performance is usually presented as $T_C$ and $P_C$ (or their negatives) versus $1/\lambda$ = tip speed/wind speed ratio, because there is always a wind speed even though the shaft speed may be zero.

When the geometry and characteristics of a minimum induced loss rotor, designed by the procedure of Section IV, are used to predict rotor performance at the design point according to the algorithms of Section V, the values of $T_C$ and $P_C$ are found to be slightly different. These differences were attributed to the fact that equations 38 and 39 caused the profile drag to influence the axial (aV) and rotational ($a'\Omega r$) components of the induced velocity. The equations were then modified to read

$$\frac{a}{1+a} = \frac{1}{4}\frac{\sigma}{F}\frac{c_\ell \cos\phi}{\sin^2\phi} \tag{38a}$$

$$\frac{a'}{1-a} = \frac{1}{4}\frac{\sigma}{F}\frac{c_\ell \sin\phi}{\sin\phi\,\cos\phi} \tag{39a}$$

which did not improve the differences for the one test case investigated; nevertheless, equations 38a and 39a are incorporated into HELICE as being simpler and conceptually more consistent.

## FUSELAGE OR NACELLE EFFECTS

To account for the rotor loading in the presence of a fuselage or nacelle which causes the average axial component of the flow (in the absence of the rotor) to have a value $\bar{u} \neq 1$ (see section IV, equation 35), equation 38 (or 38a) is rewritten

$$\frac{a}{\bar{u}+a} = \frac{1}{4}\frac{\sigma}{F}\frac{(c_\ell \cos\phi - c_d \sin\phi)}{\sin^2\phi} \text{ or } = \frac{1}{4}\frac{\sigma}{F}\frac{c_\ell \cos\phi}{\sin^2\phi} \tag{38b}$$

and the iteration equation, 47, is rewritten

$$\phi_{n_{II}} = \tan^{-1}\left|\left(\frac{\lambda}{\xi}\right)\frac{(\bar{u}+a)}{(1-a')}\right| \tag{47a}$$

Implementation of the iteration procedure for the typical case of $u < 1$ then leads to higher values of blade angle of attack and higher values of $\frac{dC_T}{d\xi}$ and $\frac{dC_P}{d\xi}$ than for $\bar{u} = 1$ as would be expected. These correspond to the "gross" loading of the rotor operating in the body flow field.

The calculation of the corresponding "net" thrust of the rotor-body combination then leads to different treatments for tractor and pusher propeller installations. For the case of a tractor propeller, the quantity $\bar{u} \neq 1$ reflects the potential flow field at the body nose which may be modeled by a

source-sink distribution along the body and rotor axis, or another more exact panel-singularity procedure. Account must then be taken (at least) of the buoyancy drag of the body arising in consequence of the axial variation of the rotor pressure field.

The buoyancy drag is given by

$$\text{Drag}_{\text{buoyancy}} = \frac{\rho}{2} V^2 \int_0^1 \Delta p \cdot \frac{dS}{dx}\, dx \qquad (54)$$

where $\Delta p$ is the overpressure due to the propeller, S is the body cross section area, and x is distance along the body axis of length L. Koning[11] gives an approximate relation for $\Delta p$ as a function of $\Delta x$ downstream and upstream of the rotor:

$$\frac{\Delta p}{\frac{\rho}{2}V^2} = \begin{cases} \frac{T_C}{2}\left\{1 - \frac{\Delta x/R}{\sqrt{1+(\Delta x/R)^2}}\right\}; & \Delta x\ (+) \\ & \text{(downstream)} \\ \frac{T_C}{2}\left\{1 - \frac{\Delta x/R}{\sqrt{1+(\Delta x/R)^2}}\right\}; & \Delta x\ (-) \\ & \text{(upstream)} \end{cases} \qquad (55)$$

A tractor propeller has comparatively little effect upon the skin friction of the body boundary layer if the boundary layer is already assumed turbulent, because a single rotation propeller is inherently incapable of increasing the axial slipstream velocities close to the axis. It is capable of imparting considerable rotational velocity to the slipstream, however, and this, in combination with the periodic injection of blade momentum wakes into the body boundary layer, will almost certainly provoke transition of an otherwise laminar boundary layer.

A pusher propeller installation also may have $\bar{u} < 1$ by reason of the body potential flow field, and the body may have buoyancy drag by virtue of the negative axial gradient of the rotor pressure in the vicinity of its tail, but the effects of the running propeller on the body boundary layer are predominantly favorable. There is a well known instance of a prototype tandem twin engine airplane which was incapable of maintaining single engine flight on its forward propeller because of the excessive drag produced by separation of the body boundary layer after the aft propeller was stopped. In the case of "pusher" steamboat propellers, operational considerations force the propeller to be made so small that it is almost entirely immersed in the hull boundary layer, and a propeller design philosophy of "erasing" the remote hull wake is adopted.

In the HELICE program the treatment of body interference is under the control of the analyst. He can readily compare the thrust and power absorption of an isolated propeller ($\bar{u} \equiv 1$) designed to absorb a certain power at a certain advance ratio with minimum induced loss loading, with the thrust and power absorption of a similar propeller "depitched" (equation 35) to support approximately the same radial loading in a known body flow field ($\bar{u} \neq 1$). The gross thrust coefficients for this depitched propeller can then be debited by a correction proportional to the gross thrust coefficient, since the body buoyancy drag and the slipstream dynamic pressure increase are proportional to $C_T$ and $T_C$. In this way, the "net" thrust of the propeller-body combination can be made equal to (or less than) the thrust of an isolated propeller at the same design point. There is very little experimental evidence to serve as a guide; indeed, almost all experimental data on actual propellers contains uncompensated body interference effects of one kind or another.

## APPLICATION

1. WAKEFIELD CLASS RUBBER POWERED MODEL AIRPLANE: Figure 4 presents the along-axis and in-plane views of a two bladed propeller capable of maintaining an initial climb angle of 27.8° for a model with a flying mass of 200 gms and an L/D of 10. The propeller has a diameter of 600 mm and turns at 480 rpm at an airspeed of 5 m/s in air with a density of 1.225 kg/m$^3$ (760 mm Hg at 15°C). Curves are also given for $C_T$, $C_P$, and n and for radial variations of $c_\ell$ with different advance ratios. Because of the low Reynolds number, the blade elements are given a minimum profile drag coefficient of 0.02, a

maximum lift coefficient of 0.9, and a value of $\frac{dc_d}{d(\alpha^2 deg)} = 0.0006$, which makes the drag coefficient 0.0416 at stall. Even so, a design point efficiency of 0.798 is calculated, and a peak efficiency of 0.823 at a slightly higher advance ratio is indicated, which would occur sometime after launch when the rubber motor was somewhat unwound and turning the propeller more slowly. Other calculations not given here suggest that such a propeller in combination with a 40 gm rubber motor would take the model to an altitude of 55 m, and that the total duration of flight -- power plus glide -- would exceed 3 minutes in still air.

2. POWERED HANG GLIDER: Figure 5 presents the same information for a propeller for a powered hang glider. The two bladed propeller is designed to absorb 7457 W (10 hp) at a shaft speed of 1946 rpm [(9/37) x 8000 crankshaft rpm] with a diameter of 1372 mm (54 inches). The airspeed is taken to be 13.41 m/s (30 mph) in sea level density air. The propeller is really much too small to absorb this much power at this airspeed. Because the tip speed is 10.4 times the flight speed, the blade chord near the tips required to support the Betz-Prandtl circulation is small, but the chord near the blade roots is immense, which might be structurally desirable. The design point efficiency is calculated to be between 0.55 and 0.62 when appropriate airfoil section data are used. The iteration procedure given in Section V refuses to converge for advance ratios much below the design point. The theory of this paper was not meant to apply to such a heavily loaded propeller.

3. SELF-LAUNCHING SAILPLANE: Figure 6 presents the propeller characteristics and Figure 7 presents the calculated performance of a self-launching sailplane fitted with a HELICE designed propeller and powered by a snowmobile engine. The engine puts out 13.42 kW (18 hp) at 6000 rpm in sea level density air. The two bladed propeller of 889 mm (35 inch) diameter is designed to absorb this power at an airspeed of 30 m/s (67 mph), and will give a rate of climb of 2.6 m/s (510 ft/min) at this speed at a flying mass of 239 kg (527 lb). At airspeeds higher than 30 m/s, the engine must be throttled to prevent overspeeding. Even so, the engine propeller combination appears to be capable of maintaining level flight at an airspeed of 43.5 m/s (97 mph) with a part throttle output of 10 kW (13.4 hp) at 6000 rpm. The high tip speeds ($\Omega R$ = 279 m/s or Ma = 0.82) help keep the blade area small to reduce the airframe drag when the propeller is stopped.

4. PEDAL DRIVEN AIRPLANE PROPELLER: Figure 8 gives the geometry performance, and radial lift coefficient distribution for a propeller similar to that used on the Chrysalis and Gossamer Albatross airplanes. This two bladed propeller is designed to absorb 373 W (0.5 hp) at a shaft speed of 125 rpm and an airspeed of 5 m/s, corresponding to steady climbing flight. Selection of a diameter of 4.267 m (14 ft) and a design point lift coefficient of 0.8 insures a climb efficiency of 0.83 and cruise efficiencies of nearly 0.90. The propeller design and performance algorithms which I wrote in an early version of this paper[12] were used by my student, Hyong Bang, to write the program used to design the Chrysalis and Gossamer Albatross airplanes. Its astonishing success led to the development of HELICE, which is more flexible in its application.

## AVAILABILITY OF HELICE

Mrs. French and I have been continually debugging HELICE since the first workable versions were available late in 1979. The discovery in the spring of 1980 that it would design minimum induced loss windmills and predict their off-design performance has led to the generalization of the "print" statements (e.g. "ROTOR" now replaces "PROPELLER") and the incorporation of certain escape modes to terminate cases without loss of previously stored information when improper operation is indicated (e.g. $a < -0.5$, corresponding to the vortex ring state). It is planned to make program listings, floppy disc

inputs, and user's manuals available through M.I.T. during the summer of 1981 at a price comparable to two programmer man weeks. Please address all inquiries to Mrs. Susan E. French, Room 41-317, M.I.T., Cambridge, MA 02139, USA.

## REFERENCES

1. Betx, A. and Prandtl, L., "Luftschrauben mit geringstem Energieverlust," Goettinger Nachrichten, 1919; also in "Vier Abhandlungen zur Aero- und Hydrodynamik," Goettingen, 1927.
2. Goldstein, S., "On the Vortex Theory of Screw Propellers," Proceedings of the Royal Society (London), Series A, Volume 63, 1929.
3. Glauert, H., "Airplane Propellers," Division L, Volume IV of Durand's Aerodynamic Theory, Springer Verlag, 1936. Also photo offset versions by Durand reprinting committee, 1942, and Dover Press.
4. Lerbs, H.W., "Moderately Loaded Propellers with a Finite Number of Blades and an Arbitrary Distribution of Circulation," translation by the Society of Naval Architects and Marine Engineers, Volume 60, 1952.
5. Theodorsen, T., "The Theory of Propellers," McGraw-Hill Publishing Co., 1948.
6. Hirsch, R., "Determination et Calcul des Helices d'Avion Optima, Simples et Coaxiales," Publications Scientifiques et Techniques du Ministere de l'Air, 1948.
7. Giordano, V., "La Circulazione per l'Elica Ottima di Betz e la Soluzione di Goldstein," L'Aerotecnica Missili e Spazio, No. 2, 1974.
8. de Vries, O., "Wind Tunnel Tests of a Two-Bladed Horizontal Axis Wind Turbine and Evaluation of an Aerodynamic Performance Calculation Method," National Lucht-en-Ruimtevaartlaboratorium report NLR TR 79071L, 1979.
9. Dunbeck, P., "Performance of Light Airplane Propellers," S.M. Thesis, Course 16, M.I.T., Febraury 1979.
10. Zimmer, J., "Wakes and Performance of Light Aircraft Propellers," S.M. Thesis, Course 2, M.I.T., June 1980.
11. Koning, C., "Influence of the Propellers on Other Parts of the Airplane Structure," Durand, Vol.IV, Div. M
12. Larrabee, E., "Design of Propellers for Motorsoarers," NASA Conf. Proceedings for the 3rd Int. Symposium on the Aerodynamics for Low Speed Flight, CP 2085, Volume I, 1979.

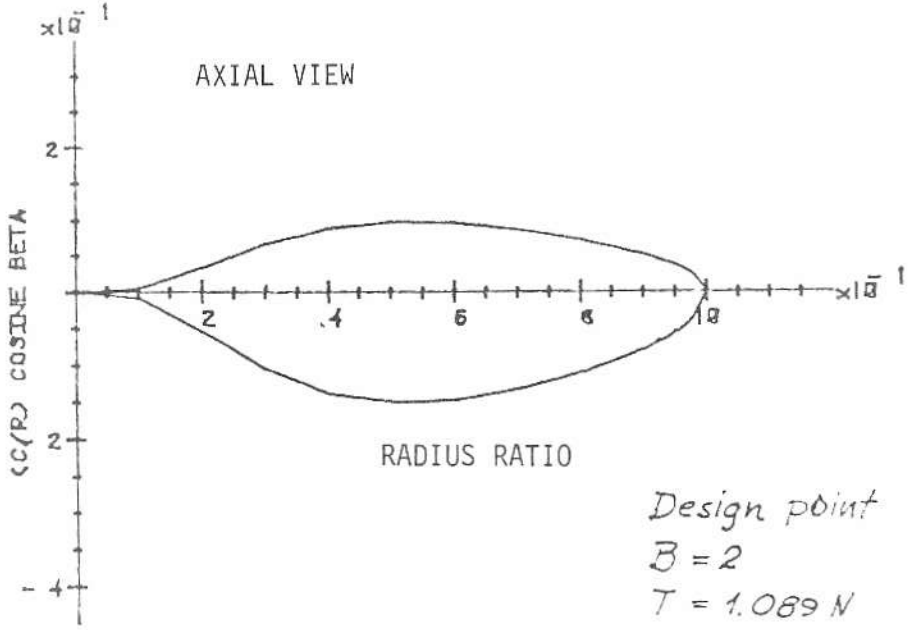


Design point
B = 2
T = 1.089 N
V = 5 m/s
460 rpm
R = 300 mm
ρ = 1.225 kg/m³

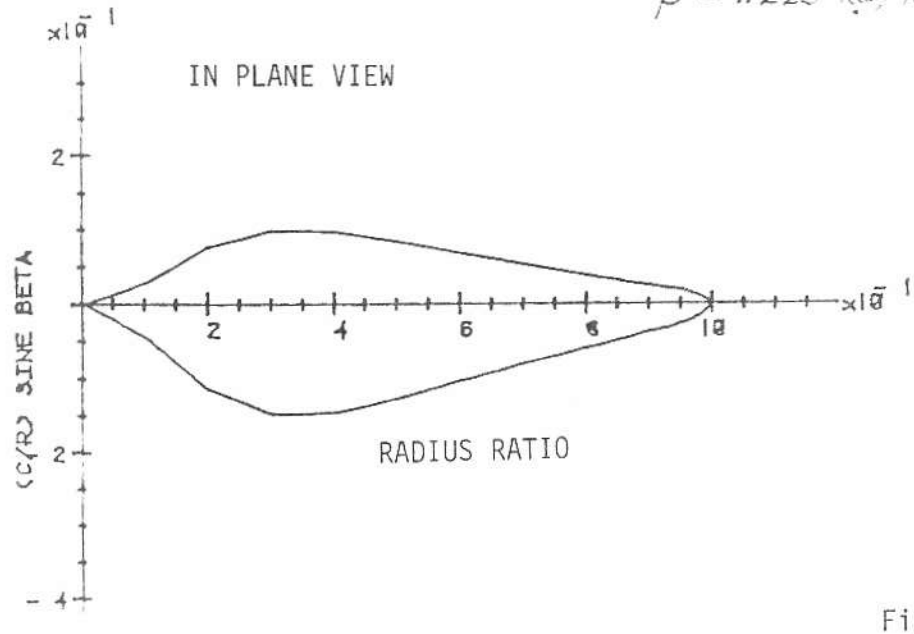


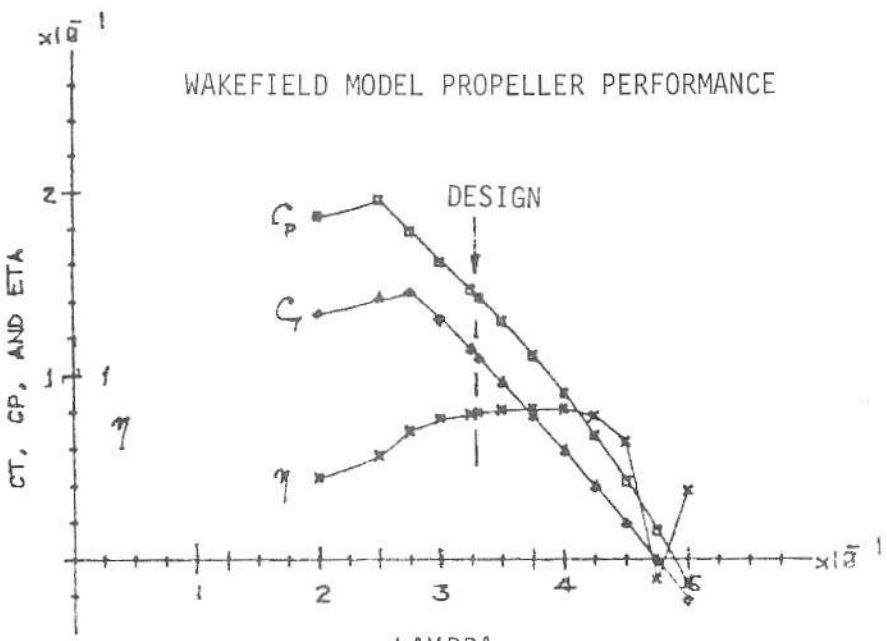


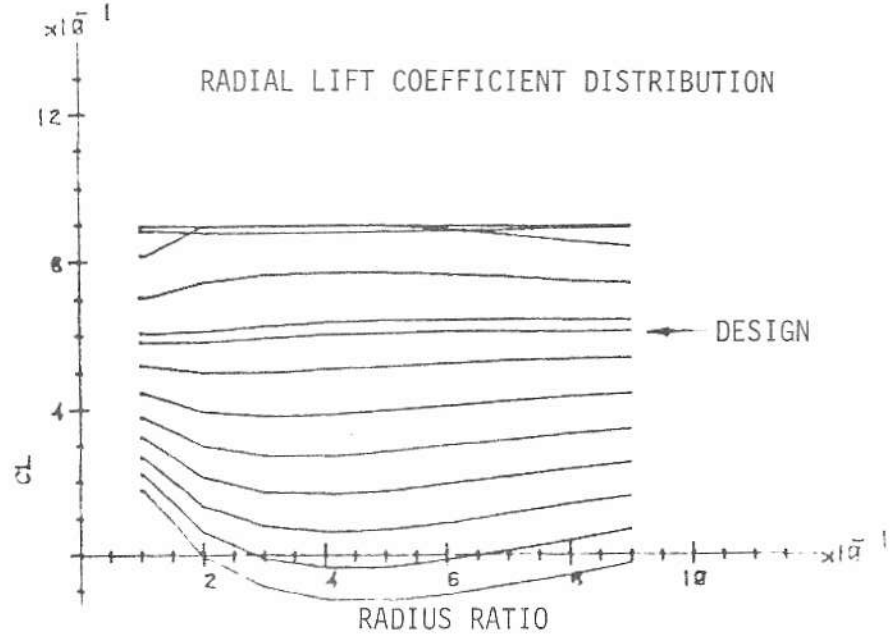


Figure 4

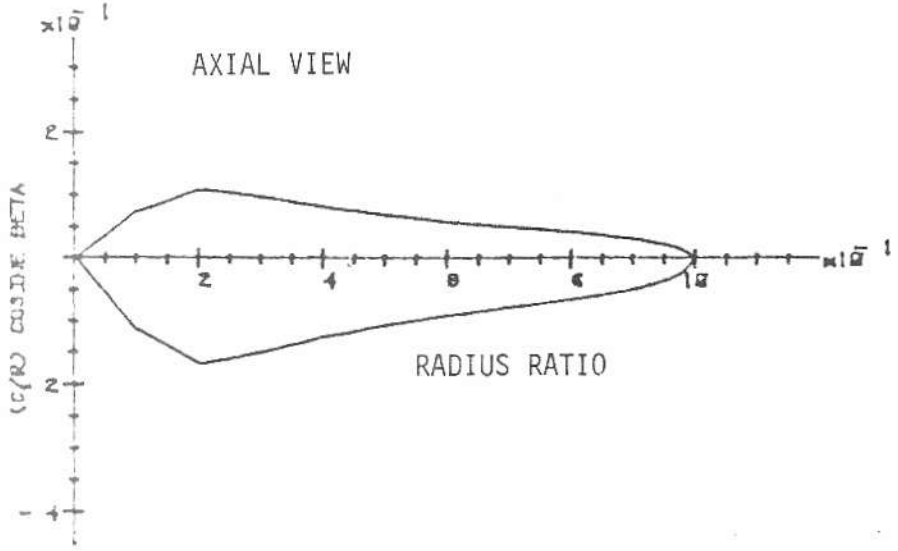


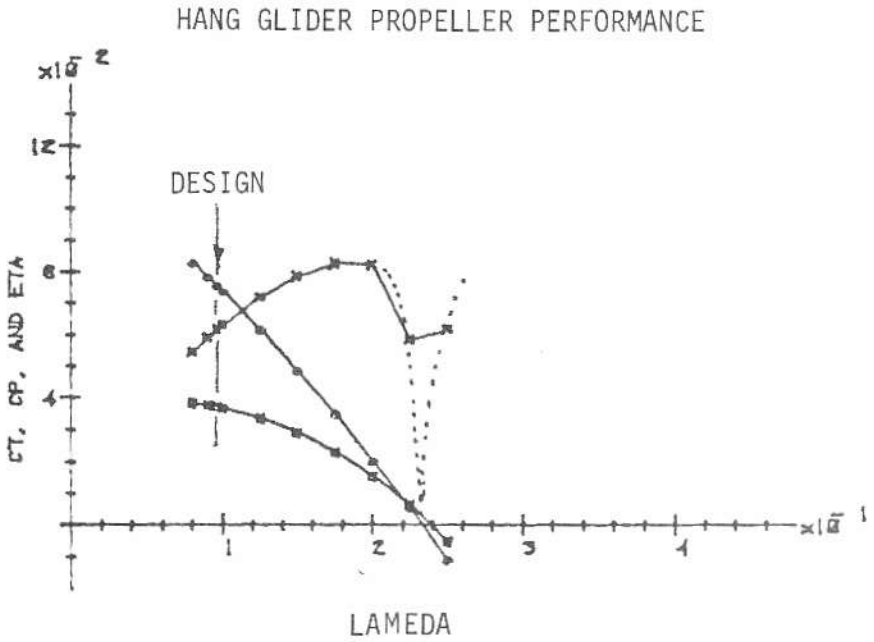


$B = 2$
$P = 7457\ W$
$V = 13.41\ m/s$
$1946\ rpm$
$R = 686\ mm$
$\rho = 1.225\ Kg/m^3$

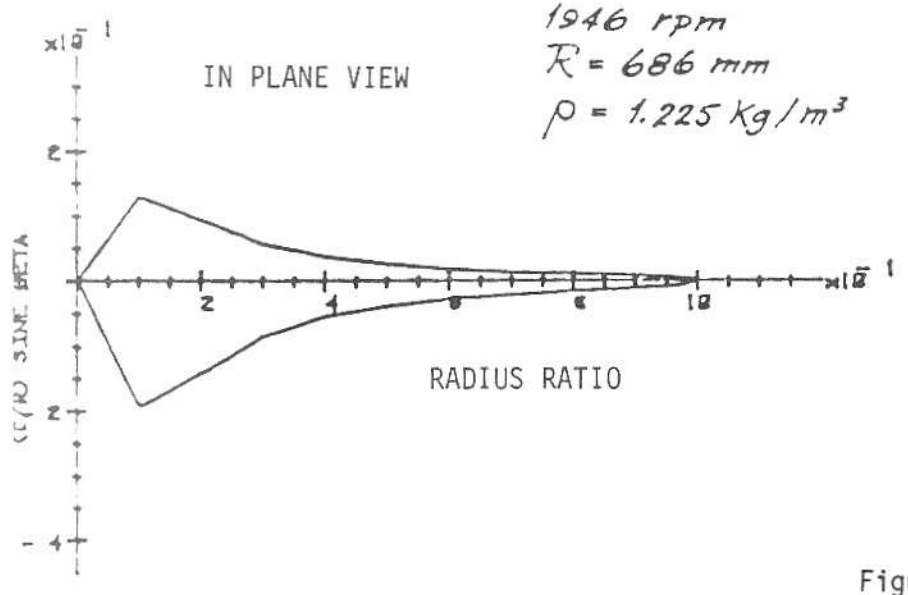


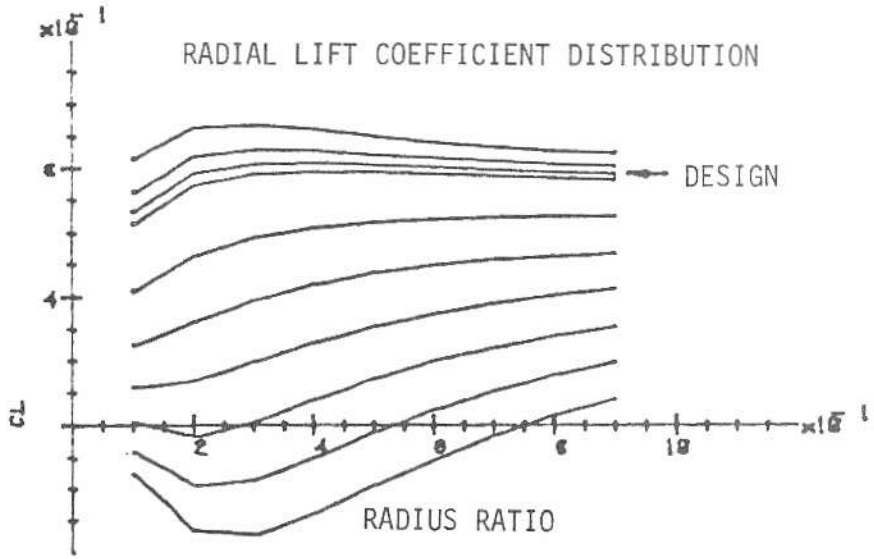


Figure 5

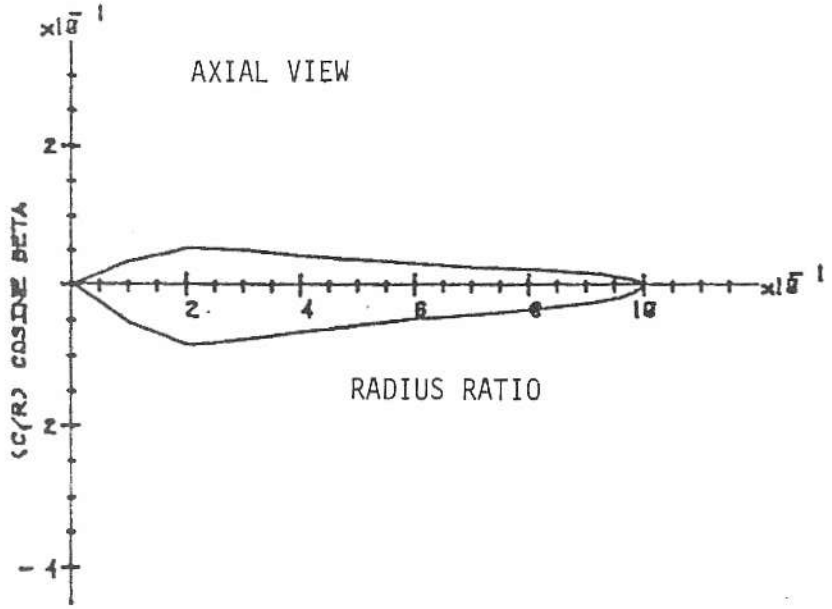


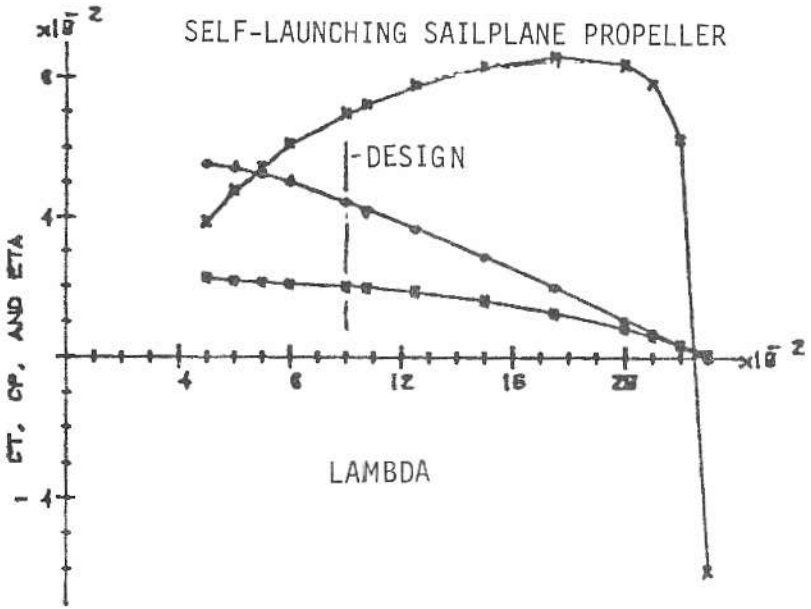


B = 2
P = 13.42 kW
V = 30 m/s
6000 rpm
ρ = 1.225 kg/m³

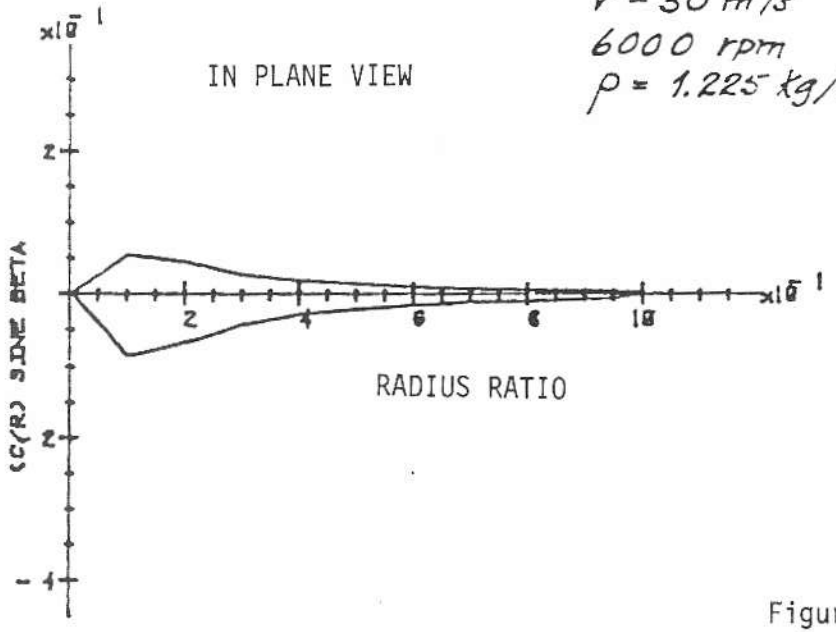


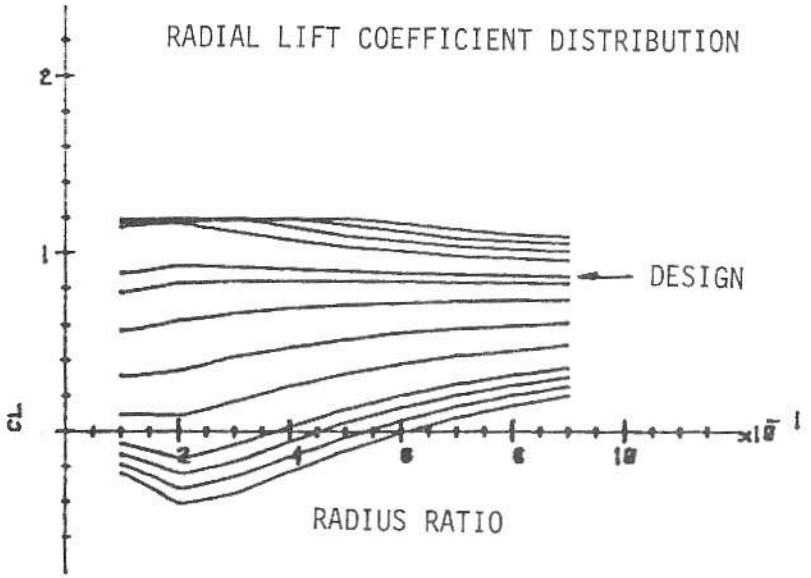


Figure 6

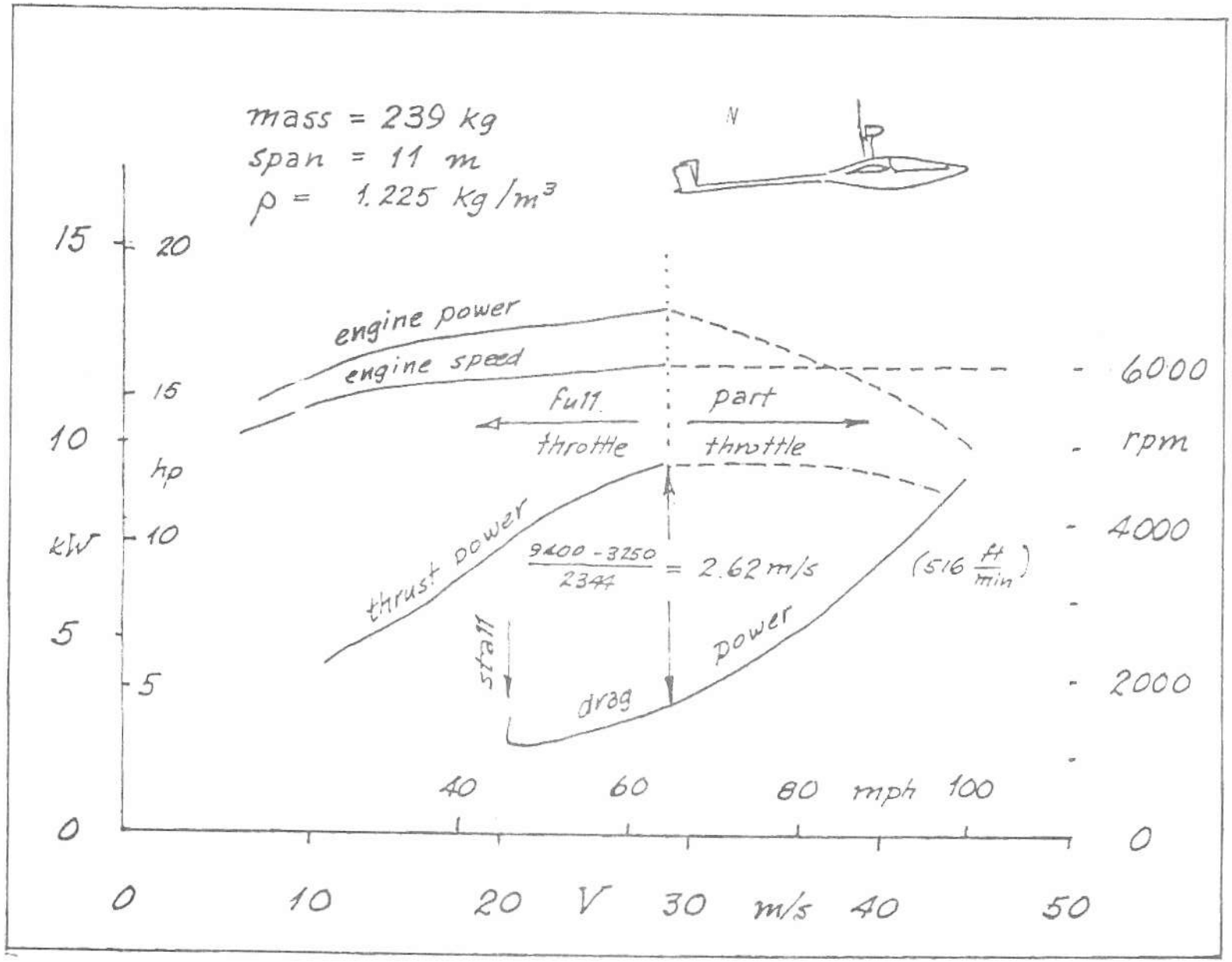


Fig. 7 Engine-propeller-airframe performance for a self launching sailplane.

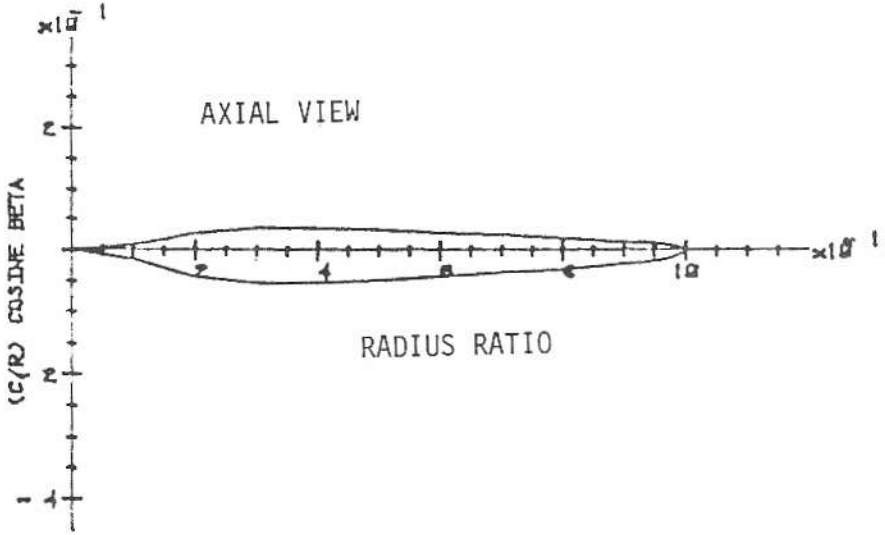


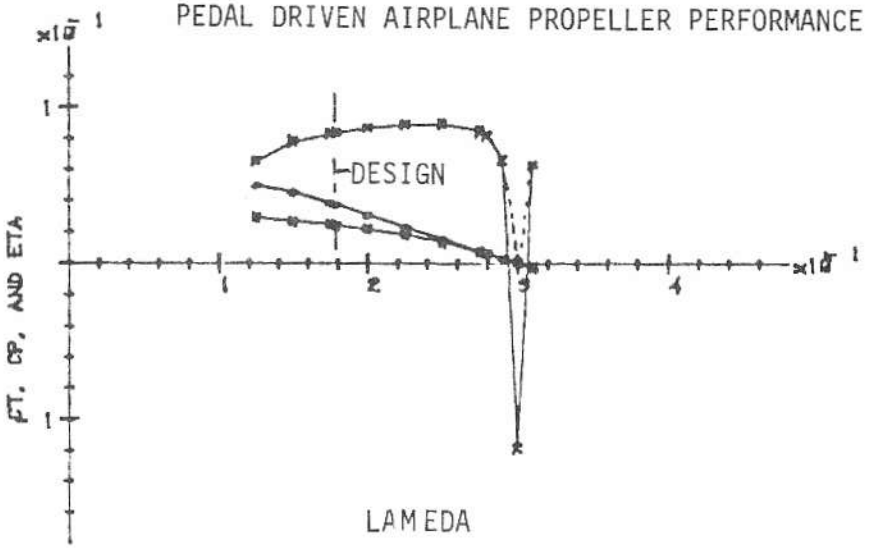


$B = 2$
$P = 373\ W$ (0.5hp)
$V = 5\ m/s$
$R = 1.1336\ m$ (7 ft)
$\rho = 1.2\ kg/m^3$
125 rpm

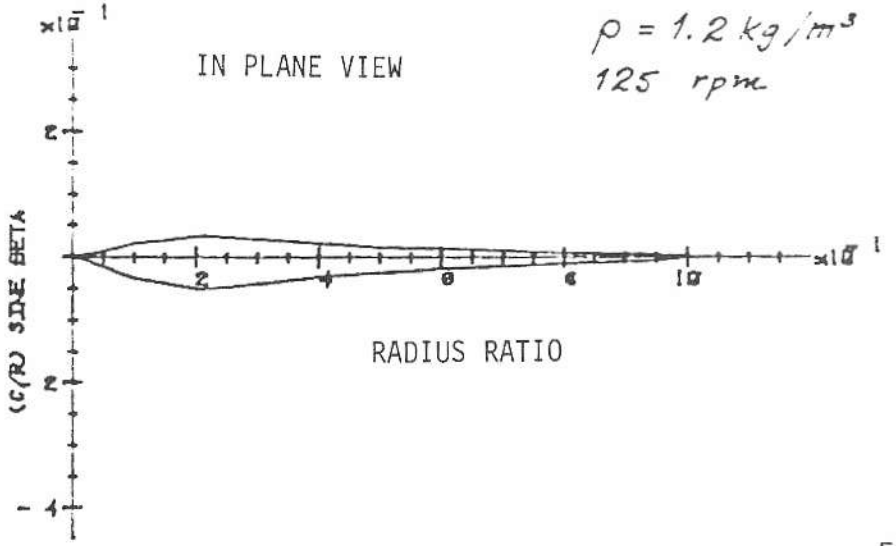


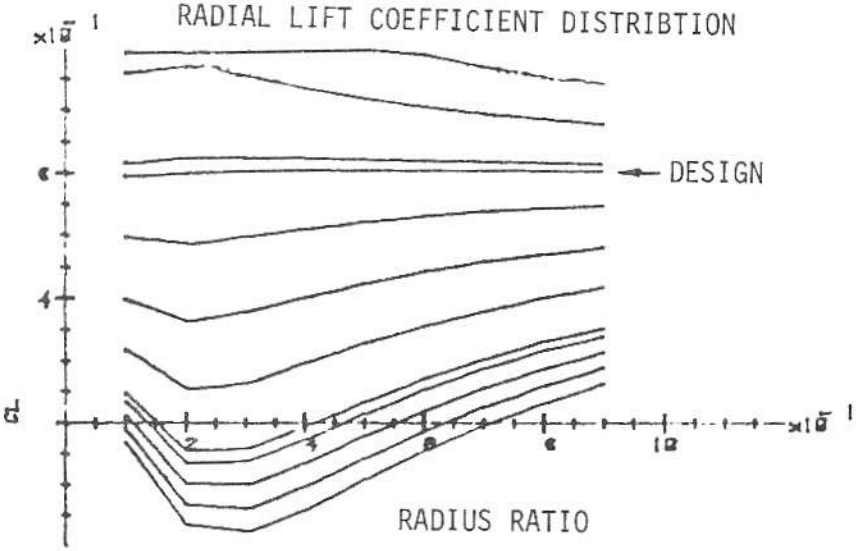


Figure 8